

Raman Images of a Single Molecule in a Highly Confined Plasmonic Field

Sai Duan,^{1,2} Guangjun Tian,² Yongfei Ji,² Jiushu Shao,³ and Yi Luo^{1,2,*}

¹*Hefei National Laboratory for Physical Science at the Microscale and Synergetic Innovation Center of Quantum Information & Quantum Physics, University of Science and Technology of China, Hefei, 230026 Anhui, P. R. China.*

²*Department of Theoretical Chemistry and Biology, School of Biotechnology, Royal Institute of Technology, S-106 91 Stockholm, Sweden.*

³*Key Laboratory of Theoretical Computational Photochemistry, Ministry of Education, College of Chemistry, Beijing Normal University, Beijing 100875, P. R. China.*

(Dated: December 3, 2024)

Under the local plasmonic excitation, the Raman images of a single molecule can now reach sub-nm resolution. We report here a description for the interaction between a molecule and a highly confined plasmonic field. It is shown that when the spatial distribution of the plasmonic field is comparable with the size of the molecule, the optical transition matrix of the molecule becomes to be dependent on the position and distribution of the plasmonic field, resulting in spatially resolved Raman image of a molecule. It is found that the resonant Raman image reflects the electronic transition density of the molecule. In combination with the first principles calculations, the simulated Raman image of a porphyrin derivative adsorbed on the silver surface nicely reproduces its experimental counterpart. The present theory provides the basic framework for describing linear and nonlinear responses of molecules under the highly confined plasmonic field.

The development of tip enhanced Raman scattering (TERS) technique has significantly increased the spatial resolution of Raman images for molecules[1–3]. Under the low temperature and ultrahigh vacuum conditions, the resolution has amazingly reached a sub-nanometer level for a porphyrin derivative adsorbed on the silver surface[3]. It is anticipated that the spatial confinement of the tip-induced plasmon has played a decisive role in achieving such a high resolution. In this case, the spatial distribution of the plasmonic field has to be comparable with the size of the molecule, even with the inclusion of possible nonlinear processes[3]. This situation presents a great challenge to the conventional theory, which always assumes that the electromagnetic (EM) field uniformly interacts with the molecule[4]. A new theory that takes into account the locality of the EM thus needs to be developed. Moreover, what a Raman image really tells about the molecular structure is another important issue that has not yet been discussed in the literature.

In this work, we have derived a theoretical framework to describe the Raman images of a molecule as observed in the TERS experiments. The interaction between the molecule and the plasmonic field is described quantum mechanically. In combination with the first principles calculations, we have successfully reproduced experimental Raman image of the porphyrin derivative adsorbed on the silver surface. It is found that within the Born-Oppenheimer (BO) approximation, the resonant Raman image reflects the density of the electronic transition between the ground and the excited states. The effects of nonlinear processes on the Raman images have also been briefly discussed.

The plasmon can be regarded as a highly confined EM field. We used the same scheme proposed by Archambault et al.[5] to describe the highly confined EM field.

Briefly, according to their theory[5], when the normalization condition

$$\int d\mathbf{r} \frac{1}{2} \left[\frac{\partial(\omega\epsilon)}{\partial\omega} + \frac{\mu_0}{\epsilon_0} \frac{\partial(\omega\mu)}{\partial\omega} \frac{|\tau|^2}{|\mu|^2} \right] |\mathbf{g}(\mathbf{r})|^2 = 1, \quad (1)$$

is applied, the total energy of classical highly confined plasmonic field could return to the form of uniform EM field in free space[6]. Here ω is the frequency of the incident laser, ϵ_0 and μ_0 (ϵ and μ) are permittivity and permeability of free space (relative permittivity and relative permeability), respectively, τ is the ratio of magnetic induction to electric field, and \mathbf{g} is a vector function corresponding to the normalized amplitude distribution of the electric field for the confined EM field. As a result, following the standard expressions of field quantization[5, 7, 8], the operator related to the vector potential is written as[6]

$$\hat{\mathbf{A}}(\mathbf{r}, t) = \sqrt{\frac{\hbar}{2\epsilon_0\omega V}} \left(\hat{a}(\mathbf{g}(\mathbf{r}))e^{i(\mathbf{k}\cdot\mathbf{r}-\omega t)} + \text{H.c.} \right), \quad (2)$$

where \hbar is the reduced Planck constant, V is the system volume, \mathbf{k} is the wave vector, \hat{a} is the annihilation operator for photon, and H.c. is the hermitian conjugate. Notice that, for specific nanostructures, \mathbf{g} can be determined by the classical Maxwell's equations[9]. Furthermore, the non-relativistic interaction Hamiltonian between electrons and highly confined plasmonic field can still be written as[7, 8, 10]

$$\hat{\mathcal{H}}' = -\frac{e}{m_e} \hat{\mathbf{A}} \cdot \hat{\mathbf{P}}, \quad (3)$$

where e and m_e are charge and mass of electron, respectively, and $\hat{\mathbf{P}}$ is the electron momentum operator.

The plasmonic frequency often falls into the visible or UV region, hence the electric dipole approximation still

holds[8]. Based on Fermi's Golden rule[8] and the commutation relation $g(\mathbf{r})\hat{\mathbf{P}} = \frac{m\epsilon}{\hbar}[\hat{\mathbf{r}}, g(\mathbf{r})\hat{\mathcal{H}}_0]$, the transition rate for the absorption between two molecular states may be expressed as[6]

$$\Gamma_{i \rightarrow f}^{abs} = \frac{\pi e^2 \omega_{fi}^2 n}{\epsilon_0 \omega V} |\boldsymbol{\epsilon} \cdot \langle \Psi_f | \hat{\mathbf{r}} g(\mathbf{r}) | \Psi_i \rangle|^2 \times \delta(E_f - E_i + \hbar\omega) \quad (4)$$

where $\hat{\mathcal{H}}_0$ is the unperturbed molecular Hamiltonian, E_f and E_i are the energies related to the final and initial molecular states $|\Psi_f\rangle$ and $|\Psi_i\rangle$, respectively, ω_{fi} is the corresponding frequency difference, $\boldsymbol{\epsilon}$ is the unit vector of electric polarization, and g is the corresponding component. Here we keep g inside the integral because the spatial distribution of the plasmonic field is comparable with the size of the molecule. As a result, the magnitude of the transition matrix could be influenced by the confined plasmon, i.e. nano-cavity plasmon (NCP). We notice that Eq. 4 can also be directly obtained from the equivalent interaction Hamiltonian $\hat{\mathcal{H}}' = -e\hat{\mathbf{r}} \cdot \hat{\mathbf{E}}$ [11] for the highly confined EM field. With BO approximation, the molecular state can be rewritten as $|\Psi\rangle = |\psi\rangle|v\rangle$, where $|\psi\rangle$ and $|v\rangle$ are electronic and nuclear components, respectively.

A linear Raman process is described by the polarizability of the molecule and it is a combination of the absorption and spontaneous emission processes. Thus, analogy to the Albrecht's theory[12], the polarizability can thus be written as

$$\alpha_{pq} = A_{pq} + B_{pq}, \quad (5)$$

where

$$A_{pq} = \frac{1}{\hbar} \langle \psi_g | \hat{\mathbf{p}} | \psi_r \rangle \langle \psi_r | \hat{\mathbf{q}} g(\mathbf{r}) | \psi_g \rangle \times \sum_{v^r=0}^{\infty} \frac{\langle v^f | v^r \rangle \langle v^r | v^i \rangle}{\omega_{e^r v^r: e^g v^i} - \omega - i\Gamma} + \text{NRT} \quad (6)$$

and

$$B_{pq} = \frac{1}{\hbar} \frac{\partial \langle \psi_g | \hat{\mathbf{p}} | \psi_r \rangle}{\partial Q_k} \langle \psi_r | \hat{\mathbf{q}} g(\mathbf{r}) | \psi_g \rangle \times \sum_{v^r=0}^{\infty} \frac{\langle v^f | Q_k | v^r \rangle \langle v^r | v^i \rangle}{\omega_{e^r v^r: e^g v^i} - \omega - i\Gamma} + \frac{1}{\hbar} \langle \psi_g | \hat{\mathbf{p}} | \psi_r \rangle \frac{\partial \langle \psi_r | \hat{\mathbf{q}} g(\mathbf{r}) | \psi_g \rangle}{\partial Q_k} \times \sum_{v^r=0}^{\infty} \frac{\langle v^f | v^r \rangle \langle v^r | Q_k | v^i \rangle}{\omega_{e^r v^r: e^g v^i} - \omega - i\Gamma} + \text{NRT}. \quad (7)$$

Here p and q are the Cartesian coordinates, $|\psi_g\rangle$ and $|\psi_r\rangle$ are the electronic ground and resonant excited states, Q_k is the corresponding normal mode, $|v^i\rangle$ and $|v^f\rangle$ are initial and final vibrational states in $|\psi_g\rangle$, $|v^r\rangle$ is vibrational

state in $|\psi_r\rangle$, $\omega_{e^r v^r: e^g v^i}$ is the frequency difference between $|\psi_r\rangle|v^r\rangle$ and $|\psi_g\rangle|v^i\rangle$, Γ is the damping factor, and NRT is the non-resonant term. We notice that the electronic part of A term in Eq. 6 is independent of Q_k , which provides a universal contribution to all normal modes. On the other hand, the derivatives in B term in Eq. 7 are related to individual Q_k , which have different values for each vibrational mode. In addition, both A and B terms are related to the position of NCP which could be described by the center of $g(\mathbf{r})$. Thus, the value of polarizability in Eq. 5 is related to the position of TERS tip. From the polarizability, the Raman intensity can be calculated directly[4, 12, 13]. According to the definition, the first order Taylor expansion for $g(\mathbf{r})$ would lead to the electric field gradient effects in Raman spectroscopy as discussed in the literature[14, 15].

We now focus our attention on the resonant Raman scattering in order to simulate the experimental Raman images. In this case, the A term in Eq. 5 becomes the dominant term[4, 12]. Moreover, for a molecule under the TERS tip, only the zz component in Eq. 6 needs to be evaluated[3]. By definition, scale function $g(\mathbf{r})$ is the amplitude distribution of the confined electric field, which represents the position of the NCP. For the sake of computations, we have chosen to expand it in terms of the Gaussian basis sets.

$$g(\mathbf{r}) = \sum_D \sum_{l,m,n} \sum_{\alpha} c_{\alpha,D}^{lmn} g_{\alpha,D}^{lmn}, \quad (8)$$

where $g_{\alpha,D}^{lmn}$ is a Gaussian function localized at the center \mathbf{r}_D with exponent α , which can be written as

$$g_{\alpha,D}^{lmn} = (x - x_D)^l (y - y_D)^m (z - z_D)^n e^{-\alpha(\mathbf{r} - \mathbf{r}_D)^2} \quad (9)$$

and $c_{\alpha,D}^{lmn}$ is the corresponding coefficient. Here \mathbf{r}_D may represent the position of the NCP. As the first demonstration, only the s -type Gaussian functions are considered for $g_{\alpha,D}^{lmn}$. It is noted that for absolute Raman intensities g should satisfy the normalization condition in Eq. 1[6]. However, for the Raman images, the relative values are adequate. For the practical calculations, we chose $c_{\alpha,D}^{lmn} = 1$ and $l = m = n = 0$ in Eq. 8. We should mention here that the quantization was adopted to describe the generation of the plasmon in a previous study for the surface-enhanced Raman scattering[16]. However, the interaction between the plasmonic field and the molecule was still treated non-locally[16]. We also notice that the current theory can be connected to the time dependent Kohn-Sham approach in real space for highly confined EM field[17].

We put the new theory to the test by directly simulating the system that was measured in a recent study[3], i.e. a single *meso*-tetrakis-(3,5-di-tertiarybutylphenyl)-porphyrin (H_2TBPP) molecule adsorbed on the silver (Ag) surface. The high resolution scanning tunneling microscope (STM) and Raman images[3] provide good

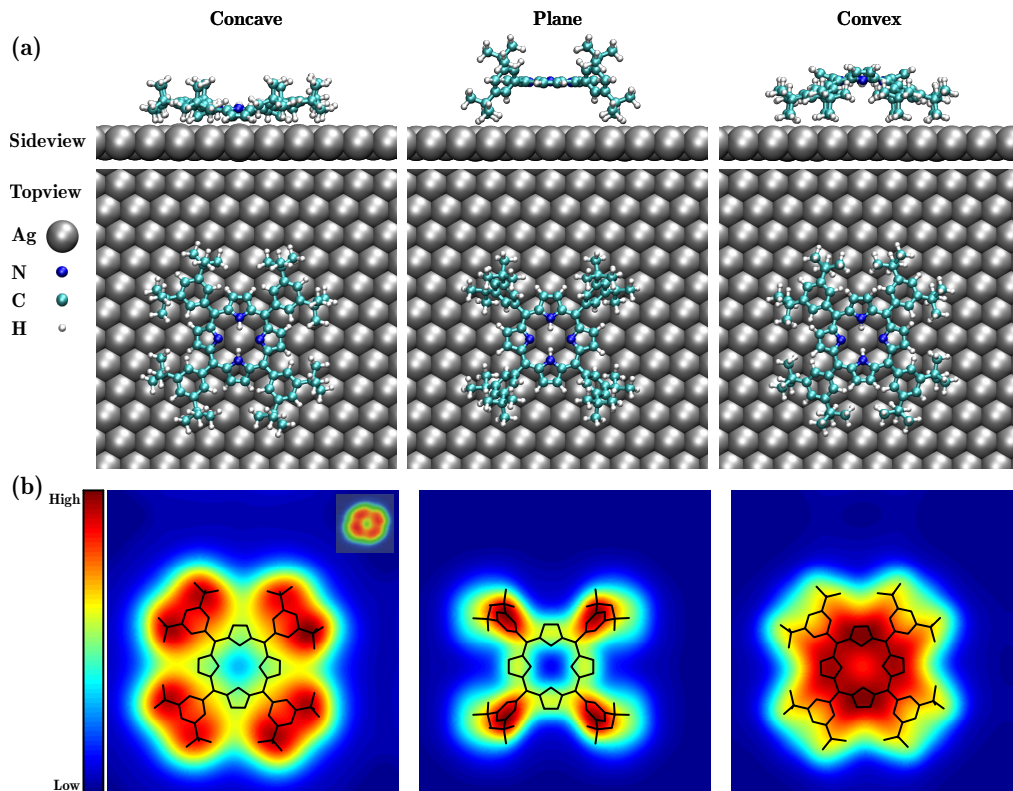


FIG. 1. (a) Optimized structures of one H₂TBPP tautomer adsorbed on the Ag(111) surface for concave, plane, and convex configurations, respectively. Gray, blue, cyan and white balls represent Ag, N, C, and H atoms, respectively. Only the topmost slab layer of the Ag(111) surface as well as all atoms of adsorbates in one supercell are depicted for clarity. (b) Calculated average STM images with the sample biased by 1.0 V for concave, plane, and convex configurations, respectively. The solid lines represent the skeleton of H₂TBPP. The insert figure shows the experimental STM image under the same condition extracted from Ref. 3.

references for theoretical modeling. The details of the density functional theory calculations are given in the Supplemental Material[6].

Here we considered two degenerate tautomers of H₂TBPP molecule[18]. The optimized structures of one H₂TBPP tautomer adsorbed on the Ag(111) surface are depicted in Fig. 1(a)[6]. The optimized structures of the other tautomers are similar except the central hydrogens bonded to different nitrogen atoms. We have considered three configurations: concave, plane, and convex, respectively. The first and last configurations were identified when H₂TBPP adsorbed on the Cu(111) surface by STM[19] and the second configuration is the minimum of the isolated molecule. Our calculations have shown that the concave is the most stable adsorption configuration, owing to the long range dispersion included in current calculations[20]. Meanwhile, the second stable configuration is the plane and the convex is the least stable one. The calculated STM images[6] of all configurations, together with the experimental result[3] are given in Fig. 1(b). One can immediately see that only the calculated STM image of the concave resembles well the experimental image. It can thus be concluded that

H₂TBPP adsorbed on the Ag(111) surface has the concave configuration under the experimental conditions.

To simulate the Raman image, H₂TBPP was extracted from the optimized adsorption structures and its excited states were calculated by the time dependent density functional theory at the hybrid B3LYP level with 6-31G(d) basis sets[6]. It should be mentioned that it is the compromise that we have to make for such large systems from computational point of view. It is fortunately a reasonable approximation since the molecule is only physisorbed on the Ag(111) surface. The strong absorption states for three configurations are found to be 2.47, 2.36, and 2.25 eV, respectively, in the region of the excitation energy of the experiment (532 nm, 2.33 eV)[3]. We have thus chosen these three excited states to simulate the resonant Raman images. Consistent with the experimental setup[3, 21], the center of NCP, i.e. \mathbf{r}_D , is in the plane which is about 2 Å above the highest position of the adsorbates. Meanwhile, along the x and y directions, the full width at half maximum (FWHM) of the plasmonic field, $g_{\alpha,D}^{000}$, was set to be 5, 10, 20, and 30 Å, respectively, while the z component was fixed at 5 Å. We should emphasize that the calculated Raman

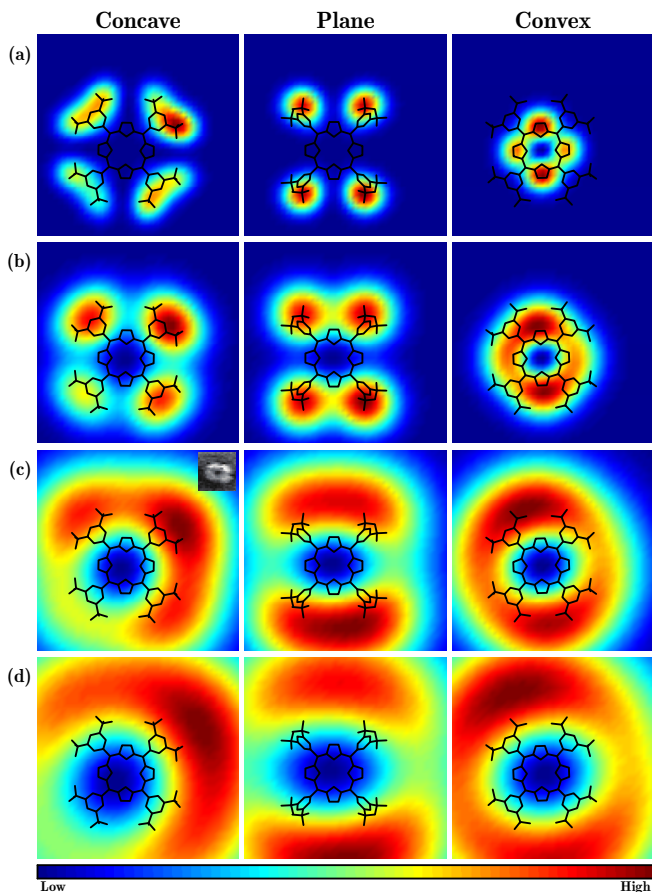


FIG. 2. Calculated Raman images with the x and y components of full width at half maximum to be (a) 5 Å, (b) 10 Å, (c) 20 Å, and (d) 30 Å for concave, plane, and convex configurations, respectively. The solid lines represent the skeleton of H_2TBPP , while, the insert figure shows the experimental Raman image extracted from Ref. 3.

images are not sensitive to small changes of \mathbf{r}_D and the α in the z component of $g_{\alpha,D}^{000}$.

All simulated Raman images are presented in Fig. 2. It can be seen that the size of the Raman image is dependent on the size of the NCP. This implies that the precondition for the high resolution Raman image is to generate a highly focused plasmonic field. It is nice to observe that different configuration of the molecule gives very different Raman image, indicating that TERS technique is a powerful tool to study the structure of adsorbates. One can notice that the Raman image of the concave with FWHM of 20 Å is in very good agreement with the experimental image, which is consistent with the energy and STM calculations. Here the symmetry breaking of the calculated Raman images should be attributed to the interaction between adsorbates and the Ag(111) substrate. By definition, Raman images reflect the density change involved in the electronic transition, rather than the local density of state of the adsorbate. This is naturally reflected by the obvious difference between the

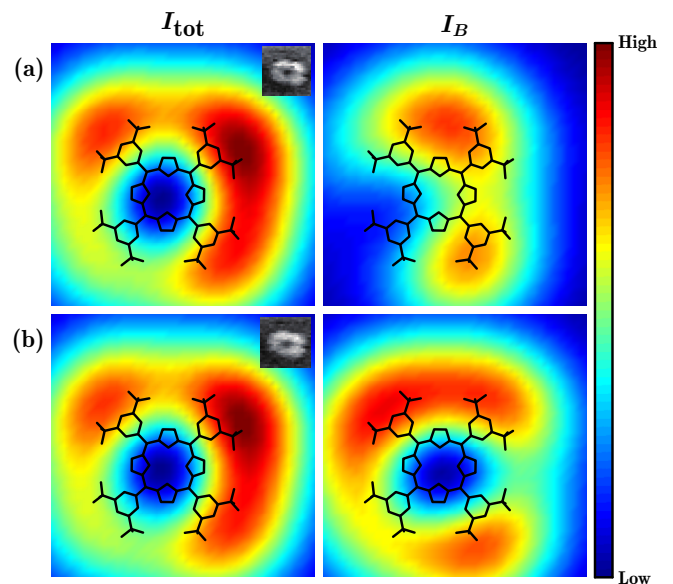


FIG. 3. Calculated Raman images of two bands at (a) 820 cm^{-1} and (b) 1200 cm^{-1} from total polarizability (I_{tot}) and only the B term (I_B) with the full width at half maximum of 20 Å for the concave configuration. The I_B was scaled by a factor of 100 and 400 for 800 and 1200 cm^{-1} , respectively. The solid lines represent the skeleton of H_2TBPP , while, the insert figures are the corresponding experimental Raman images extracted from Ref. 3.

Raman and STM images.

Under the resonant condition, the B term often gives a small contribution to the total intensity. We have evaluated numerically the effect of the B term for two vibrational bands, around 820 and 1200 cm^{-1} , by using the linear coupling model[22]. The calculated Raman images from the total polarizability as well as the B term alone for these two bands are shown in Fig. 3. One can immediately notice that the B term is very sensitive to the vibrational models. Its contribution to the total intensity holds the key to distinguish Raman images of different vibrations. For the H_2TBPP molecule, the contribution of the B term is very small. Hence, the Raman images from total intensity calculations appear to be identical for two vibrational bands. It should be mentioned that the Raman calculations are performed for the single molecule. The inclusion of the substrate could increase the contribution of the B term. This could be a reason behind the small variation observed in the experimental Raman images[3]. We would like to note that in Ref. 3 the so-called calculated Raman images were represented directly by the spatial distribution of vibrational modes. However, according to the basic theory presented in this work, those calculated images have no direct connections to what were observed experimentally

As mentioned before, the calculated linear Raman image with FWHM of 20 Å can reproduce the experimental observations very well. Although the theoretical limit for

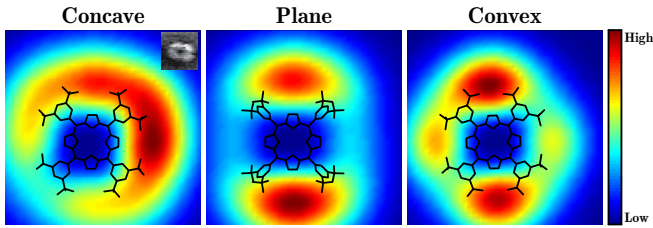


FIG. 4. Calculated nonlinear Raman images for concave, plane, and convex configurations, respectively, under the plasmonic field with the full width at half maximum of 20 Å. The solid lines represent the skeleton of H₂TBPP, while, the insert figure shows the experimental Raman image extracted from Ref. 3.

the size of the field is 1 Å[23, 24], it is generally assumed that the actual size of the confined plasmonic field could be larger than 20 Å. The possible involvement of nonlinear processes was thus suggested to be the key for the utilization of sub-nm resolution Raman images[3], since it can provide the same results that a plasmonic field with much reduced spatial size can offer. We have to admit that we are not at the position yet to derive a rigorous theory for the stimulated Raman and other nonlinear processes[25, 26] under a highly confined plasmonic field. However, we can nevertheless estimate the effects of the nonlinearity on the Raman images by simply assuming that it is the cubic of the absolute value of the polarizability as suggested by Zhang et al.[3]. The calculated nonlinear Raman images with the FWHM of 20 Å are depicted in Fig. 4. In general, the nonlinear images have slightly higher spatial resolution than their linear counterparts. It seems like that the inclusion of the nonlinear effects does give a better agreement between the calculated and the experimental images.

In summary, we have proposed a quantum mechanical description for the interaction between a molecule and a highly confined plasmonic field. It shows that the NCP could modify the transition matrix and result in the Raman images with high resolution. The usefulness of the description is highlighted by reproducing successfully the experimental Raman images of a H₂TBPP molecule adsorbed on the Ag(111) surface. The theoretical framework established in this work lays the foundation for the future development of linear and nonlinear plasmonic spectroscopy.

This work was supported by Ministry of Science and Technology of China (Grant No. 2010CB923300), Natural Science Foundation of China (21121003, 21161160557), Strategic Priority Research Program of Chinese Academy of Sciences (XDB01020200), Göran Gustafsson Foundation for Research in Natural Sciences

and Medicine, and the Swedish Research Council. The Swedish National Infrastructure for Computing (SNIC) was acknowledged for computer time.

* yiluo@ustc.edu.cn

- [1] R. M. Stöckle, Y. D. Suh, V. Deckert, and R. Zenobi, *Chem. Phys. Lett.* **318**, 131 (2000).
- [2] B. Pettinger, B. Ren, G. Picardi, R. Schuster, and G. Ertl, *Phys. Rev. Lett.* **92**, 096101 (2004).
- [3] R. Zhang, Y. Zhang, Z. C. Dong, S. Jiang, C. Zhang, L. G. Chen, L. Zhang, Y. Liao, J. Aizpurua, Y. Luo, J. L. Yang, and J. G. Hou, *Nature* **498**, 82 (2013).
- [4] D. A. Long, *The Raman Effect: A Unified Treatment of the Theory of Raman Scattering by Molecules* (Wiley, Chichester New York, 2002).
- [5] A. Archambault, F. Marquier, J.-J. Greffet, and C. Arnold, *Phys. Rev. B* **82**, 035411 (2010).
- [6] See Supplemental Material for theoretical background and computational details.
- [7] R. Shankar, *Principles of Quantum Mechanics*, 2nd ed. (Plenum Press, New York, 1994).
- [8] N. Zettili, *Quantum Mechanics: Concepts and Applications*, 1st ed. (Wiley, Chichester New York, 2001).
- [9] J. D. Jackson, *Classical Electrodynamics*, 3rd ed. (Wiley, New York, 1998).
- [10] M. Blume, *J. Appl. Phys.* **57**, 3615 (1985).
- [11] M. O. Scully and M. S. Zubairy, *Quantum Optics*, 1st ed. (Cambridge University Press, Cambridge New York, 1997).
- [12] A. C. Albrecht, *J. Chem. Phys.* **34**, 1476 (1961).
- [13] J. Neugebauer, M. Reiher, C. Kind, and B. A. Hess, *J. Comput. Chem.* **23**, 895 (2002).
- [14] J. K. Sass, H. Neff, M. Moskovits, and S. Holloway, *J. Phys. Chem.* **85**, 621 (1981).
- [15] E. J. Ayars, H. D. Hallen, and C. L. Jahncke, *Phys. Rev. Lett.* **85**, 4180 (2000).
- [16] D. J. Masiello and G. C. Schatz, *Phys. Rev. A* **78**, 042505 (2008).
- [17] T. Iwasa and K. Nobusada, *Phys. Rev. A* **80**, 043409 (2009).
- [18] Q. Fu, J. Yang, and Y. Luo, *App. Phys. Lett.* **95**, 182103 (2009).
- [19] S. Ditze, M. Stark, F. Buchner, A. Aichert, N. Jux, N. Lucas, A. Görling, W. Hieringer, J. Hornegger, H.-P. Steinrück, and H. Marbach, *J. Am. Chem. Soc.* **136**, 1609 (2014).
- [20] S. Grimme, *J. Comput. Chem.* **27**, 1787 (2006).
- [21] X. H. Qiu, G. V. Nazin, and W. Ho, *Science* **299**, 542 (2003).
- [22] P. Macak, Y. Luo, and H. Ågren, *Chem. Phys. Lett.* **330**, 447 (2000).
- [23] U. Kreibig and M. Vollmer, *Optical Properties of Metal Clusters* (Springer, Berlin New York, 1995).
- [24] J. M. Atkin and M. B. Raschke, *Nature* **498**, 44 (2013).
- [25] Y. R. Shen, *The Principles of Nonlinear Optics*, 1st ed. (Wiley-Interscience, Hoboken, N. J, 2002).
- [26] S.-Y. Lee, D. Zhang, D. W. McCamant, P. Kukura, and R. A. Mathies, *J. Chem. Phys.* **121**, 3632 (2004).